dc electric field effect on the microwave properties of $YBa_2Cu_3O_7/SrTiO_3$ layered structures

A. T. Findikoglu, C. Doughty, S. M. Anlage, Qi Li, X. X. Xi, and T. Venkatesan
Center for Superconductivity Research, Department of Physics, University of Maryland, College Park, Maryland 20742

(Received 21 March 1994; accepted for publication 23 May 1994)

We present a summary of our work on the dc electric field effect on the microwave properties of $YBa_2Cu_3O_7/SrTiO_3$ (YBCO/STO) layered structures. We briefly describe the fabrication of these layered structures, their structural and electrical properties related to the microwave response, and experimental methods to investigate dc electric field effects at microwave frequencies. Analysis of microwave measurements shows that dc electric field modulated changes in both the complex conductivity of YBCO layers and the dielectric properties of the STO layers contribute to the overall device response. At low temperatures (<50 K) and large electric fields, good samples show linear gate-voltage modulation of microwave surface resistance and surface reactance attributable to field induced superconducting hole filling and depletion in the dominant YBCO layer.

I. INTRODUCTION

When an electric field is applied perpendicular to the surface of a material, the mobile carrier density at the surface changes. If the material is thin enough, then the modulation of the carrier density at the surface induces appreciable changes in the transport properties of the material. This effect is the basis of field-effect transistors (FETs). Electric field effects can also be used to investigate the basic electrodynamic properties of materials through the reversible modulation of carrier densities.

Recently, low-frequency measurements on the electric field effect in $YBa_2Cu_3O_7$ (YBCO) thin films using YBCO/$SrTiO_3$(STO) layered structures have shown appreciable modulation of normal and superconducting properties of YBCO, such as normal state resistivity,[1,2] critical current density,[3] kinetic inductance,[4] and critical transition temperature.[5,6] Various research groups have also been investigating the prospects of utilizing these effects for FET-like device structures.[7,8]

A technologically attractive extension of the low frequency field effect device concept is to use it at microwave frequencies so that microwave surface impedance (Z_s), i.e., surface resistance (R_s) and/or surface reactance (X_s), can be electrically modulated.[9] It has already been demonstrated that, at least in some cases, passive devices made from metal-oxide superconductors can have superior performance to those made from conventional metals such as Au or Cu.[10] The use of active superconducting microwave devices together with the existing passive superconducting devices may create new opportunities for novel systems applications. Active device applications of electric field effect in superconductor-dielectric layered structures may include variable attenuators, tunable phase shifters, tunable oscillators, and resonators.[9]

From a basic science point of view, measurements of electric field induced changes in Z_s, in principle, provide information about the field modulation of the density of carriers in both the normal and superconducting channels, simultaneously. Depending on the design of the measurement apparatus, one can measure these changes in a broad range of temperatures, easily covering the critical transition temperature (T_c) of the superconductor. Additionally, with certain assumptions, one may determine important physical parameters[11] such as the surface carrier mobility of normal carriers, the effective mass of superconducting carriers, and the carrier density dependence of the critical transition temperature T_c.

However, unlike dc or low-frequency experiments, measurements at microwave frequencies will also sample the high-frequency characteristics of the gate dielectric and the gate electrode. Knowledge of the relative magnitude of the effects due to the superconducting channel, dielectric gate, and normal or superconducting gate electrode is important in not only accurately determining the physical parameters of interest, but also in assessing the potential for constructing useful devices based on the electric field effect.

For the dc electric field effect studies, one essentially needs a parallel-plate capacitor with one conducting plate as the active channel and the other conducting plate as the gate. The dielectric medium between the active channel and the gate serves as electrical isolation and allows the application of large electric fields perpendicular to the surface of the active channel. However, as described above, at microwave frequencies the distinction between the active channel and the gate becomes blurred since the field induced changes in the properties of the active channel, the dielectric medium, and the gate all contribute to the overall microwave response with varying magnitude depending on the details of the geometry, electrical properties of the layers, and the microwave field distribution. Therefore, within the scope of this paper, we will refer to this capacitor as a trilayer and define the dc electric modulation effects in terms of the effective microwave Z_s of the trilayer.

In the following, we will present the results of our experiments concerning the dc electric field effect on the microwave properties of Au/STO/YBCO and YBCO/STO/YBCO trilayers with different geometries and electrical properties. The electric field effect is investigated by applying a dc voltage between the top Au or YBCO, and the bot-

 0021-8979/94/76(5)/2937/14/$6.00

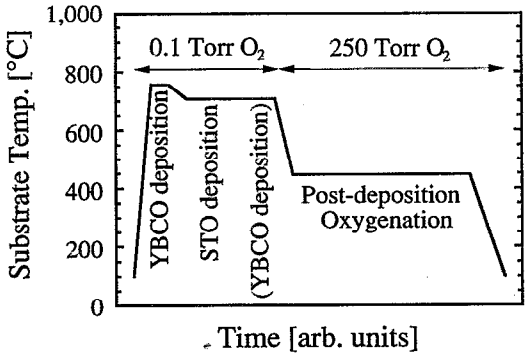

FIG. 1. Pulsed laser deposition (PLD) and *in situ* post-deposition oxygenation process for the fabrication of $YBa_2Cu_3O_7/SrTiO_3/YBa_2Cu_3O_7$ (YBCO/STO/YBCO) and STO/YBCO multilayer films.

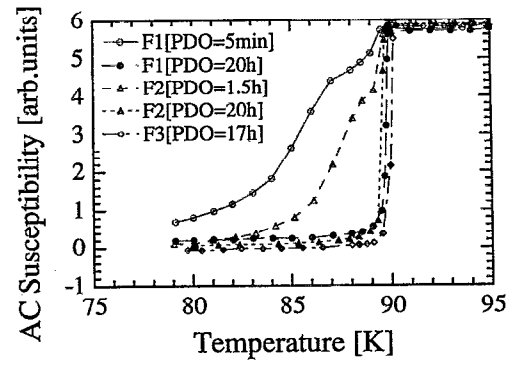

FIG. 2. ac susceptibility (in-phase) data for three $Sr_2AlTaO_6/YBa_2Cu_3O_7$ (SAT/YBCO) bilayers showing the enhancement of the superconducting transition temperature with post-deposition oxygenation (PDO) performed at 450 °C and 250 Torr oxygen. All three bilayers have thicknesses ~80 and ~800 nm for the YBCO and SAT layers, respectively. Open and full circles are for sample F1 after 5 min and 20 h of PDO, respectively. Open and full triangles are for sample F2 after respectively 1.5 h and 20 h of PDO. Open diamond data are for sample F3 with 17 h of PDO.

tom YBCO layers. Due to rather demanding sample requirements for these experiments, we begin with a description of sample preparation and determination of their general characteristics. Since we have used a new microwave measurement technique, we also discuss the novel features and limitations of this technique used for the study of dc electric field modulation effects. The body of the paper is then devoted to the analysis of the modulated microwave response, and the investigation of relationships between this response and electrical properties of the samples.

II. SAMPLE PREPARATION AND PROPERTIES

The YBCO and STO layers were deposited on (001) $LaAlO_3$ substrates by pulsed laser deposition (PLD).[12] The YBCO/STO layered structures were prepared *in situ* in a multi-target vacuum chamber using laser parameters of 248 nm wavelength, 10 Hz pulse frequency, and 1–2 J/cm^2 energy density at the target. STO targets were prepared by pressing and sintering commercially obtained STO powder (99.9% purity by weight). YBCO targets (99.9% or higher purity by weight) were obtained from several companies. The use of denser YBCO targets has given us better control over and reduction in particulate density in the films. The deposition rate was ~1 Å/pulse for both YBCO and STO layers.

The PLD and *in situ* oxygenation process for the preparation of the YBCO/STO/YBCO trilayer samples (or, similarly of the STO/YBCO bilayer samples with the exception of the top YBCO layer deposition) is shown in Fig. 1. The $LaAlO_3$ substrates were heated to 780 °C in 100 mTorr flowing oxygen. The YBCO/STO/YBCO trilayers were deposited in-situ at substrate temperatures of 720–780 °C. The nominal film thicknesses were between 40 and 80 nm for YBCO, and 0.1 and 0.8 μm for STO layers. X-ray analysis indicated that YBCO and STO grew epitaxially with the c-axis oriented normal to the substrate plane. Following the PLD process, our films were slowly cooled to ~450 °C in ~250 Torr oxygen ambient. The films were kept at this temperature and oxygen pressure for as long as 48 h to allow enough oxygenation in the bottom YBCO layer by means of slow diffusion of oxygen through the STO layer. The effect of this post-deposition oxygenation process on the bottom YBCO film properties in the case of a similar structure formed by Sr_2AlTaO_6(SAT)/YBCO bilayer, where the SAT thickness is 0.8 μm, is illustrated in Fig. 2. SAT is chemically and structurally related to STO, and shows almost identical properties to STO in terms of optimum deposition conditions.[13] We see that the transition temperature of the bottom YBCO layer gets sharper with increasing duration for post-deposition oxygenation (PDO) at 450 °C and 250 Torr oxygen. For PDO>15 h, we obtain transition temperature T_c and width ΔT_c above 89 K and less than 0.5 K, respectively, indicative of uniform optimum oxygenation for the bottom YBCO film. Using the ac susceptibility results shown in Fig. 2 and the dependence of T_c on the oxygen content in the YBCO film,[14] we obtain an upper-bound of the order of 10^{-13} cm^2/s for the oxygen diffusion coefficient in the SAT film at 450 °C.

For YBCO/STO/YBCO trilayers, the top YBCO layer was patterned by wet etching to form a 0.5–1.0 cm^2 circular capacitor plate. In the case of STO/YBCO bilayers, Au was thermally evaporated through a metal mask in a separate chamber to form the top Au capacitor plate, thus forming the Au/STO/YBCO trilayers. The Au capacitor plate had similar lateral dimensions as the patterned YBCO.

The low frequency (~1 kHz) dielectric properties of the STO layers were investigated through capacitance measurements by an LCR meter, using the bottom YBCO and the top Au or YBCO layers as capacitor plates. The critical transition temperature of YBCO layers were determined by 2-probe dc, and ~10 kHz ac susceptibility measurements. Current leakage through the STO layers under dc voltage bias were measured with an electrometer, and also a voltage source and an ammeter.

Due to strong sample dependence of the measured quantities and the difficulty in determining the intrinsic physical parameters of interest from the microwave measurements, we will concentrate on a set of three different samples and characterize them electrically as completely as possible in order to establish some correlation between the low-frequency properties and the modulated microwave response.

TABLE I. The nominal thicknesses t_{top}, t_{int}, and t_{bot} for the top, intermediate, and bottom layers, respectively; critical transition temperature onset T_c and transition width ΔT_c for the YBCO layers, and zero dc-bias relative dielectric constant ϵ_r for the STO layers of the three trilayer samples S1, S2, and S3 at 25 and 300 K.

Sample ID	t_{top} [nm]	t_{int} [nm]	t_{bot} [nm]	$T_{c\text{-top}}(\Delta T_c)$ [K]	$T_{c\text{-bot}}(\Delta T_c)$ [K]	ϵ_r @25 K	ϵ_r @300 K
S1	10 (Au)	800 (STO)	80 (YBCO)	···	80 (10)	650	300
S2	80 (YBCO)	800 (STO)	40 (YBCO)	85 (2)	88 (1)	1300	350
S3	10 (Au)	100 (STO)	80 (YBCO)	···	89 (1)	200	250

Some properties of the three samples (S1, S2, and S3) are listed in Table I, and relative thicknesses of the layers are illustrated in Fig. 3. Sample S1 is representative of our earlier samples where no post-deposition oxygenation was performed after the STO/YBCO film deposition (see Fig. 1). We believe that the relatively low T_c of the YBCO layer is due to insufficient oxygenation of this layer during cool-down.[14] The dielectric constant (ϵ_r) of the STO layer for this sample increases by a factor of ~2 when the sample is cooled from room temperature to 25 K (Fig. 4). The second sample S2 was prepared using the whole process shown in Fig. 1. The deposition and post-deposition oxygenation processes were optimized to yield smooth surfaces with minimal chemical reaction at the YBCO-STO interfaces. The sharp transition (~1 K) at ~88 K for the bottom YBCO layer shows that it is sufficiently oxygenated and there are no severe reaction problems at its interface with the intermediate STO layer. The dielectric constant (ϵ_r) of the STO layer for sample S2 increases by a factor of ~4 when the sample is cooled from room temperature to 25 K (Fig. 4). This increase, though significantly smaller than that of bulk STO single-crystals, shows that STO layer in this sample is closer to single crystalline quality than the STO layer in S1. The lower T_c of ~85 K and wider transition width of ~2 K for the top YBCO layer are most probably due to the reduced deposition temperature we used to avoid interface reaction with the intermediate STO layer.[15] As will be described later, the poorer quality of the top YBCO layer is an asset which will help us distinguish its microwave response from that of the bottom YBCO layer. The STO/YBCO bilayer in sample S3 was prepared in a similar fashion as S2 including the post deposition oxygenation process. However, the STO layer was ~8 times thinner, and the top Au was thermally evaporated in a separate chamber at room temperature. The sharp transition (~1 K) at ~89 K for the bottom YBCO layer is again indicative of good quality. The low ϵ_r of the thin STO layer and its different temperature dependence compared to thicker STO layers such as the ones in S1 and S2 (Fig. 4) might be due to unrelieved stress in the relatively thin STO film.[16]

When a dc voltage is applied between the top and bottom conducting layers of a trilayer, a dc electric field is induced in between. As a result, charge carriers of opposite polarity are accumulated at the top and bottom surfaces of the conducting layers facing the intermediate dielectric medium. Also, a leakage current flows through the dielectric medium due to nonideal insulating characteristics of the dielectric. The leakage current through the dielectric layer may lead to heating of the sample, and it also carries information about the properties of the dielectric and its conductor inter-

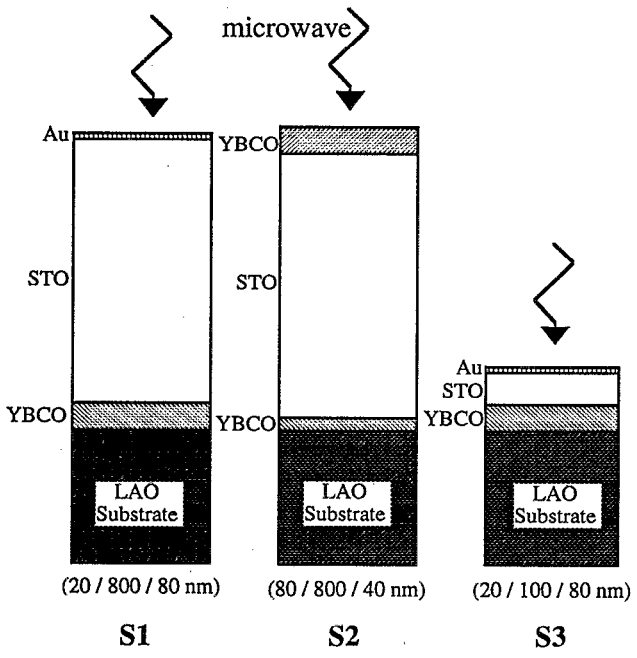

FIG. 3. Schematic of the three samples S1, S2, and S3, showing relative thicknesses for YBCO, STO, and Au layers (not drawn to scale).

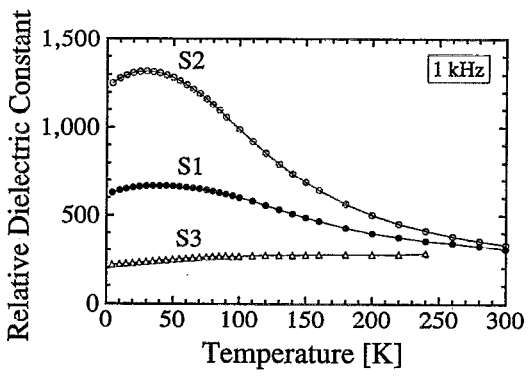

FIG. 4. Relative dielectric constant ϵ_r as a function of temperature for three trilayer samples S1 (full circle), S2 (open circle), and S3 (open triangle).

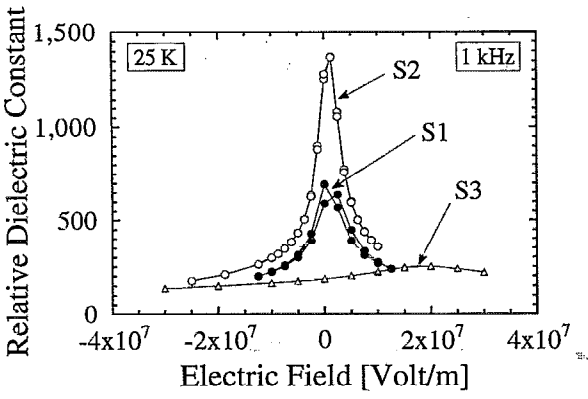

FIG. 5. Relative dielectric constant ϵ_r as a function of applied dc electric field at 25 K for three trilayer samples S1 (full circle), S2 (open circle), and S3 (open triangle).

faces. Capacitance measurements of the trilayer determine the magnitude of charge accumulation per applied voltage bias. Thus, it is important to investigate the resistivity, i.e., leakage current, and the effective dielectric constant, i.e., capacitance, of the intermediate dielectric medium as a function of dc bias and temperature. For all our dc bias experiments in this article, the top layer was grounded and the gate voltage was applied to the bottom layer.

The low-frequency (~1 kHz) dielectric properties of the STO layers were measured by using the bottom layer, and the circular top layer as capacitor plates. The circular top plates for all three samples had an area of ~0.8 cm^2. The thickness for STO and YBCO layers are given in Table I and Fig. 3. The results of the capacitance measurements on samples S1, S2, and S3 as a function of temperature and dc bias voltage (V_{dc}) are summarized in Figs. 5 and 6, respectively. We observe that the higher the ϵ_r of the dielectric, the more electric field sensitive it is. The samples with thicker STO layers, i.e., S1 and S2, have stronger temperature and electric field dependence attributable to higher film crystallinity. On the other hand, S3 shows a weaker field dependence and its dielectric constant ϵ_r decreases slightly with decreasing temperature. We have observed qualitatively the same dc bias dependence well above the superconducting temperature of the YBCO film(s), from which we conclude that the dc voltage effect in ϵ_r is not directly related to the changes in the superconducting properties. All three samples exhibit their maximum ϵ_r at 1–2 V dc bias. This offset in the symmetry point is clearly seen in Fig. 5 for sample S3 with "thin" STO layer as ϵ_r is shown as a function of electric field. We are not sure of the origin of this large built-in voltage drop in our trilayer samples. Hirano *et al.* have attributed similar offset values they have measured on their Au/STO/YBCO samples to the difference in work functions between Au and YBCO.[17] It is also interesting to note that the STO layer in S1, which was prepared without post-deposition oxygenation shows measurably large electrical hysteresis (see Fig. 5). This suggests that charge trapping sites may be related to oxygen deficiency.

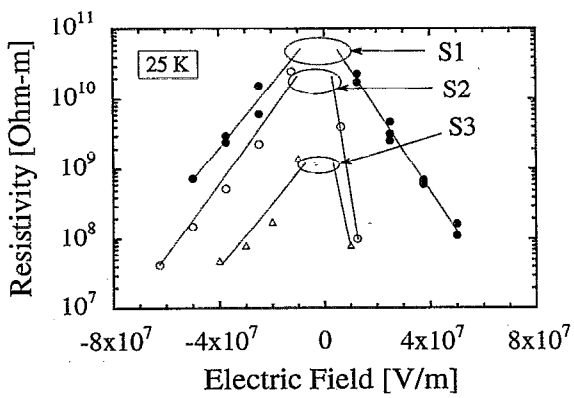

FIG. 6. Resistivity as a function of applied dc electric field at 25 K for three trilayer samples S1 (full-circle), S2 (open-circle), and S3 (open-triangle).

Figure 6 shows the dc electric field dependence of the resistivity of STO layers in samples S1, S2, and S3 at 25 K. It is rather difficult to define a breakdown electric field for these samples since they roughly show exponential decrease of resistance with bias. In the case of sample S1, at a resistivity value of 10^8 Ω m, we obtain the dielectric constant, electric field product $\epsilon_r E \sim 10^{10}$ V/m for both bias polarities. It translates into an induced surface charge density of $\sim 10^{14}$ (electrons or holes)/cm^2 at the conductor surfaces. This value might be considered to be the maximum surface charge density practically achievable with our existing technology. We also note that while the resistivity of STO in S1 where the top layer is Au shows more or less symmetric bias dependence, that of STO in S2 where the top and bottom layers are both YBCO drops significantly faster under positive bias. These results might indicate that the electric breakdown in our STO films are dominated by the bulk of the STO layer, i.e., the stress or anisotropic grain distribution in the film, rather than by the electrode type.[18]

III. DIELECTRIC RESONATOR TECHNIQUE

We have used a dielectric resonator technique to investigate the effect of dc electric field on the microwave response of YBCO/STO/YBCO and Au/STO/YBCO trilayers. This technique was briefly discussed in an earlier publication.[9] A similar technique has also been used by Klein *et al.* for the characterization of single layer YBCO films.[19] A cross-sectional schematic view of the experimental setup is shown in Fig. 7. In this technique, a sapphire puck with 4.5 mm diameter and 2.2 mm height is placed on top of the trilayer that forms an end plate of a cylindrical copper cavity. When this loaded dielectric resonator is excited in the $TE_{01\delta}$ mode at ~24.7 GHz, strong circulating currents parallel to the substrate plane are induced in the trilayer. As a result, the response of the cavity is dominated by the trilayer sample. The microwave Z_s of the trilayer is modulated by the dc gate voltage V_{dc} applied between the top and bottom conducting layers using In/Au and In contacts made to them outside the cavity. The whole assembly including the dc bias lines is attached to the cold finger of a continuous-flow cryostat where the sample can be cooled down to 8 K. Microwave measurements are performed in the unloaded coupling re-

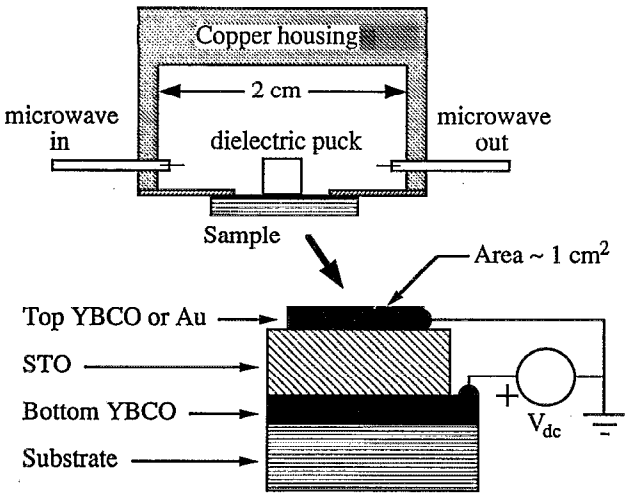

FIG. 7. Cross-sectional view of the dielectric resonator setup (not drawn to scale).

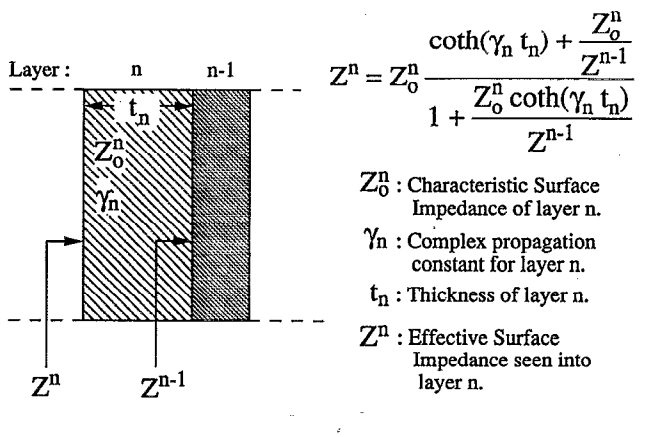

FIG. 8. Recursive model to calculate the effective surface impedance of multilayer films.

gime (achieved by adjustable coupling loops) in order to avoid complications due to external circuitry loading on the resonance.

The measured quality factor (Q) is inversely proportional to the microwave energy dissipation induced in the trilayer, i.e., to the effective surface resistance R_s. Similarly, the resonant frequency (f_0) is inversely related to the penetration of microwave fields into the sample, i.e. to the effective surface reactance X_s. In general, changes in Q and f_0 can be related to those in the effective surface impedance Z_s of any multilayer structure provided that the microwave electric and magnetic fields can be assumed to be parallel to the surface. In a quasi-TEM (transmission electron microscope) approximation with $X_{geo} \gg R_s$ and X_s, where X_{geo} is the geometric reactance of the dielectric resonator, we have[9]

$$Q \sim \frac{X_{geo}}{R_s}, \tag{1}$$

$$\frac{\delta Q}{Q} \sim \frac{\delta X_s}{X_{geo}} - \frac{\delta R_s}{R_s} \sim -\frac{\delta R_s}{R_s}, \tag{2}$$

$$\frac{\delta f_0}{f_0} \sim -\frac{1}{2}\frac{\delta X_s}{X_{geo}}, \tag{3}$$

where X_{geo} is the geometric reactance of the dielectric resonator. From independent measurements, we find $X_{geo} \sim 400\ \Omega$ at a frequency of ~24.7 GHz. This value is a factor of about 4 larger than what we estimated before.[9] Nevertheless, since we will be mostly interested in relative magnitude of the effects and fractional changes in the physical parameters, this geometric factor appears only as a scaling factor and thus does not have a significant effect on the results. In the case of electric field effects on the microwave response of our trilayer samples, the fractional changes in Q and f_0 we would like to resolve will be 1 part in $\sim 10^3$–10^4 and $\sim 10^6$–10^7, respectively. These stringent requirements will be achieved by paying close attention to thermal stability and stray electromagnetic field isolation, and also using extensive averaging.

For a multilayer system where the electrodynamics is local, i.e., electromagnetic field penetration into the individual layers can be approximated by complex exponentials, one can define the effective Z_s of the multilayer in terms of the characteristic impedance (Z_0), propagation constant (γ), and the thickness (t) of each layer. Figure 8 illustrates a simple approach to determine the effective Z_s of such a multilayer system. By iteration of the basic formula given in Fig. 8 four times, we can write a full expression for the effective Z_s of our trilayer samples in terms of the physical parameters of the individual layers and the substrate. In the analysis of our microwave measurements, we treat the medium behind the substrate essentially as an ideal infinite medium with $Z_0 \sim 377\ \Omega$ since we use a vacuum gap and a microwave absorber behind the substrates during the measurements. Therefore, under ideal circumstances where the physical parameters of the individual layers of a trilayer system are known or definable, we can establish the relation between these physical parameters, and the measured quantities Q and f_0. We have used numerical methods to investigate how the changes in the individual layer electrical properties such as conductivity and dielectric constant influence the effective microwave Z_s of the trilayers. The results of such analysis will be presented in the next chapter where appropriate. Yet, due to our limited knowledge on the microwave properties of the STO films and their interfaces, we will find this formalism to be of limited value in making a precise determination of the dc modulation effects in our trilayer samples.

IV. MICROWAVE MEASUREMENT RESULTS

In this section, we will present the results of our microwave measurements. Sample dependence will be emphasized since each sample shows fairly distinct microwave characteristics in terms of their temperature and electric field dependence. A semi-quantitative analysis of the microwave results will be given in the next section.

A. General characteristics

Some relevant low-frequency electrical properties of these three samples are given in Table I. As shown in Fig. 3,

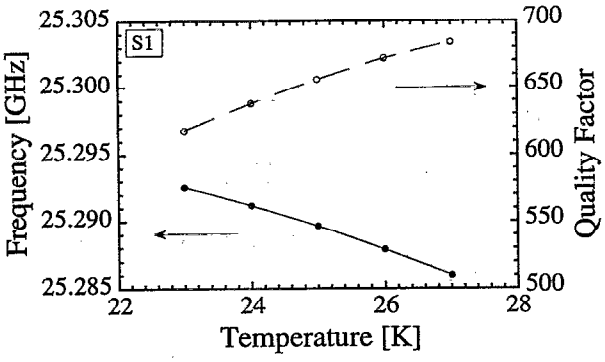

FIG. 9. Resonant frequency and quality factor vs temperature for sample S1 (lines are guide to the eye).

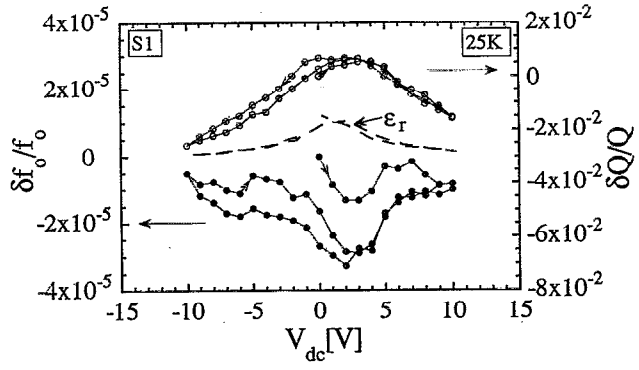

FIG. 10. Fractional changes in the resonant frequency and quality factor vs applied dc voltage V_{dc} for sample S1 at 25 K (solid lines are guide to the eye, arrows indicate direction of measurement sequence). The dashed line represents the relative dielectric constant ϵ_r in arbitrary units measured at ~1 kHz (cf. Fig. 5).

sample S1 has a "thin" (~20 nm) Au layer at the top, a rather "thick" (~800 nm) STO intermediate layer which shows electrical hysteresis in its dielectric constant, and a poorly oxygenated bottom YBCO layer which shows a reduced transition temperature and a broad transition. These factors will combine to make this trilayer very lossy, and the microwave response to be dominated by semiconductor-like losses in the intermediate STO layer, and probably in the bottom YBCO layer. Sample S2, on the other hand, has YBCO as the top layer with a thickness (~80 nm) almost half the zero-temperature magnetic penetration depth, and again "thick" intermediate STO layer. This configuration leads to comparable effects of both the top YBCO and the intermediate STO layers on the microwave response. The last sample S3 represents a configuration where the top Au and the intermediate STO layers are "thin" (20 and 100 nm, respectively). As a result, the microwave modulation will be strongly influenced by the changes in the complex conductivity of the bottom YBCO layer at a broad range of temperatures and electric fields.

For all three samples, the top layer is grounded and the dc bias is applied to the bottom YBCO film. For samples S1 and S3, the effect of dc electric field on the "thin" top Au layer is expected to be negligible compared to that on the bottom YBCO layers since the density of carriers in Au is >10 larger than that in YBCO.[20] The measurement time spent between any two consecutive microwave data points for all f_0 and Q shown in the following is ~30 s. Thus, time resolution of modulation effects in the microwave measurements will be limited to >30 s.

B. Sample S1

Figure 9 shows the Q and f_0 of the dielectric resonator loaded by sample S1 as a function of temperature. The measured Q for this trilayer is more than an order of magnitude smaller than what we measure for a quality single layer YBCO film with a similar YBCO thickness.[21] In other words, the effective surface resistance R_s is at least an order of magnitude larger. The increase of Q with temperature (i.e., semiconductor-like behavior) and also the fact that f_0 decreases while Q increases suggests that the microwave losses in the trilayer are not dominated by metallic losses.

Figure 10 and 11 illustrate the effect of dc electric field on the effective microwave Z_s of sample S1. This effect manifests itself through small changes in f_0 and Q of the dielectric resonator. As a quick inspection of Eqs. (2) and (3) will reveal, the fractional changes in f_0 are expected to be much smaller than those in Q mainly because, due to the choice of the dielectric resonator design, the geometric reactance X_{geo} which dominates the total reactance of the dielectric resonator is much larger than the effective surface resistance R_s of the trilayer which dominates the total loss. At relatively low dc bias voltages (±10 V), Q decreases whereas f_0 increases, indicating lower R_s and higher X_s, in either polarity with an offset of ~2 V for the symmetry point. The electrical hysteresis becomes measurably large especially for negative bias. These results are strongly correlated with the voltage bias induced changes in the low-frequency capacitance of the trilayer shown in Fig. 5. Figure 11 shows the dc bias effect at larger voltages (±40 V). Large electrical hysteresis loops appear more or less symmetrically around the origin, with a significant reduction of Q and an increase of f_0 compared to zero bias initial condition. There

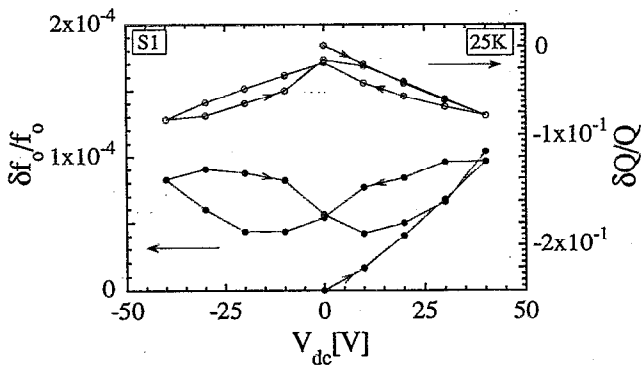

FIG. 11. Fractional changes in the resonant frequency and quality factor vs applied dc voltage V_{dc} for sample S1 at 25 K for larger voltage biases (solid lines are guide to the eye, arrows indicate direction of measurement sequence).

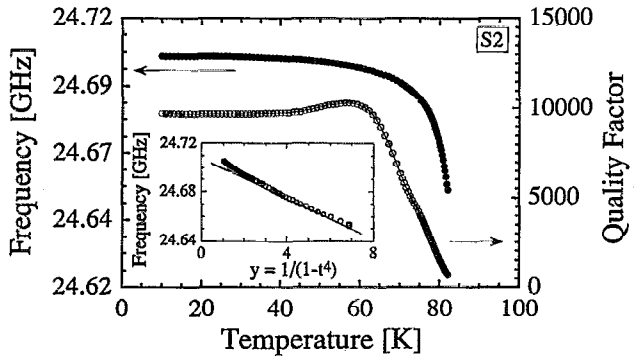

FIG. 12. Resonant frequency and quality factor vs temperature for sample S2. Inset shows the frequency as a function of $y=1/(1-t^4)$, where t is the reduced temperature given by $t=T/85$ K.

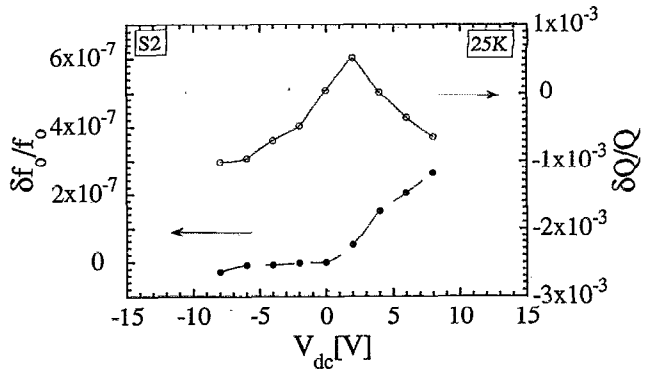

FIG. 13. Fractional changes in the resonant frequency and quality factor vs applied dc voltage V_{dc} at 25 K for sample S2 (solid and broken lines are guide to the eye).

is no remnant change in Q and f_0 at zero-voltage bias. Also, we were not able to detect any temperature hysteresis even for high voltage biases. Different paths we followed in the voltage-temperature phase space did not yield any appreciable hysteresis, either. These results together with the low-frequency results indicate that the measured electrical hysteresis is not related to ferroelectricity.[22]

C. Sample S2

This sample represents a trilayer where the electric field modulated microwave response, under certain conditions, is dominated by the top superconducting layer. For this sample, the breakdown voltage was +10 and −50 V for the forward and reverse biases, respectively.

Figure 12 shows the Q and f_0 of the resonator as a function of temperature. The decrease of f_0 with temperature for the trilayer is similar to what we expect for a single layer YBCO film with a $T_c\sim85$ K and a thickness of 80 nm.[23] Thus, we conclude that the top YBCO layer dominates the frequency shift, i.e., the total reactance change. Q of this sample at low temperatures is more than a factor of 10 larger than that of the previous sample S1, and is within a factor of 2 of what we measure for a single layer YBCO film with comparable film thickness. However, the nonmonotonic changes in Q are quite different from the monotonic decrease of Q with temperature we measure for a single layer YBCO film well below T_c.[24] Using the experimental data shown in Fig. 12 and Eq. (1), we obtain $R_s\sim30$ mΩ for the trilayer at 25 K and 24.705 GHz.

The inset to Fig. 12 shows that the frequency shift is roughly linear with $y=1/(1-t^4)$ where $t(=T/T_c)$ is the reduced temperature and $T_c\sim85$ K. This behavior is consistent with the predictions of a simple 2-fluid model.[25] The thin film limit yields $X_s[t]\alpha\lambda^2[t]\sim\lambda^2[0]/(1-t^4)$, where $\lambda[t]$ is the magnetic penetration depth at reduced temperature t. Thus, we obtain

$$X_s[t]\sim\frac{X_s[0]}{(1-t^4)}. \tag{4}$$

Using the linear fit shown in the inset to Fig. 12 and Eqs. (3) and (4), we obtain the effective surface reactance for the top YBCO layer $X_{sy}\sim250$ mΩ at 25 K. From the frequency shift data, we observe that the contribution of the STO layer and the bottom YBCO layer to the total surface reactance is negligible or unobservable. Thus, for the sake of simplicity, we will make a crude approximation and assume $X_s\sim X_{sy}$ (in other words, we will assume that the total effective surface reactance is dominated by the surface reactance of the top YBCO film).

Figure 13 illustrates the fractional change in the frequency f_0 and quality factor Q produced by the trilayer at 25 K and low dc bias voltages (±8 V). Q decreases with applied voltage in both polarities with a small offset. This response is correlated with the measured low frequency ϵ_r decrease, and may thus originate from the changes in the dielectric properties of the STO layer. Figure 14 shows the effect of dc voltage on a wider range (−50 to +10 V) on both the low frequency dielectric constant ϵ_r and the microwave response. For low dc bias, we observe that changes in ϵ_r are correlated with the changes in Q. However, below ~−10 V, the changes in ϵ_r of the STO saturate, and we believe that in this region the changes in the conductivity of the top YBCO layer dominate the microwave response. With

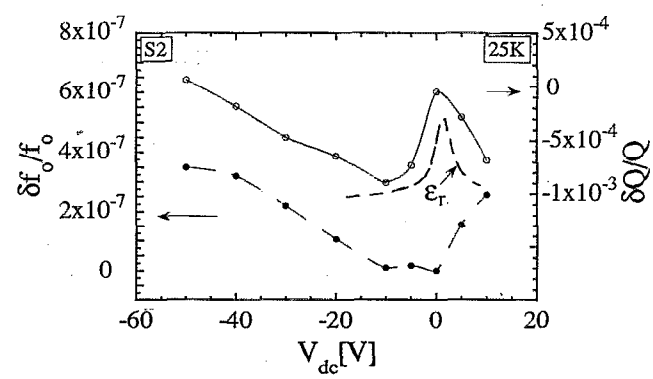

FIG. 14. Fractional changes in the resonant frequency and quality factor vs applied dc voltage V_{dc} at 25 K for sample S2 for larger voltage biases (solid and broken lines are guide to the eye). The dashed line represents the relative dielectric constant ϵ_r in arbitrary units measured at ~1 kHz (cf. Fig. 5).

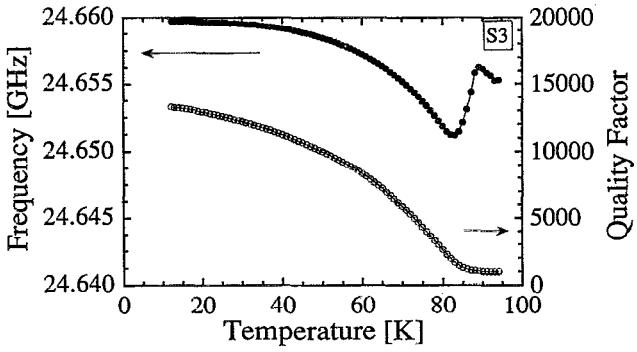

FIG. 15. Resonant frequency and quality factor vs temperature for sample S3.

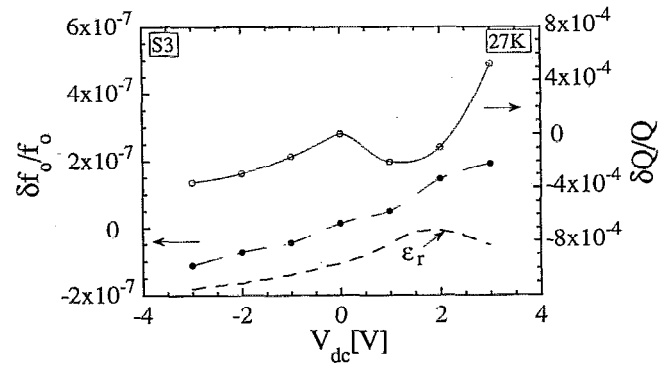

FIG. 16. Fractional changes in the resonant frequency and quality factor vs applied dc voltage V_{dc} at 27 K for sample S3 (solid and broken lines are guide to the eye). The dashed line represents the relative dielectric constant ϵ_r in arbitrary units measured at ~1 kHz (cf. Fig. 5).

voltage bias decreasing below −10 V, which corresponds to adding holes to the top YBCO layer, both Q and f_0 increase linearly.

D. Sample S3

Sample S3 represents a trilayer where the only YBCO layer in the system dominates the changes in the microwave response for a wide range of temperatures and electric fields. Temperature dependence of the resonant frequency f_0 and the quality factor Q is shown in Fig. 15. We can clearly distinguish 3 distinct regimes in this figure; a region (T <82.5 K) where both the resonant frequency f_0 and the quality factor Q decrease with increasing temperature, another region (82.5 K<T<89 K) where the resonant frequency f_0 increases while the quality factor Q decreases, and a third region (T>89 K) where neither the resonant frequency f_0 nor the quality factor Q changes appreciably with temperature. The overall behavior is consistent with the predictions of standard superconductivity theories and can be explained easily within the framework of a simple 2-fluid model in the thin film limit:[25,26] at temperatures much below the transition temperature T_c, the surface reactance X_s of the superconducting YBCO layer is larger than the surface resistance R_s mainly because there are more carriers in the superconducting channel than there are in the normal channel, and as the temperature increases R_s increases and X_s decreases because increasingly more charge carriers go from the superconducting channel into the normal channel. At a certain temperature close to the transition temperature T_c, the surface resistance R_s becomes equal to the surface reactance X_s. The exact position of this temperature depends on the physical parameters of the superconducting layer such as inertia of carriers and electronic scattering rate, and of the electromagnetic interaction such as the excitation frequency. It also depends on the surface density of normal carriers in the parallel conducting channel formed by the Au layer. Experimentally, this temperature corresponds approximately to the temperature where the resonant frequency f_0 is a minimum. In a region between this resonant frequency minimum (~82.5 K) and the transition temperature T_c (~89 K), decreasing the density of superconducting carriers in the system leads to a decrease in the surface reactance X_s (i.e., an increase in f_0), and an increase in the surface resistance R_s (i.e., a decrease in Q). Above the transition temperature T_c, all the charge carriers are essentially in the normal state. Thus above T_c, as expected, we see that the microwave response is relatively constant. We attribute the measurably high quality factor Q for this sample even in the normal state to the relatively low extrinsic losses in the trilayer, and the existence of a parallel conducting channel formed by the Au layer. The details of this argument will be presented in the next analysis section.

Figure 16 shows the dc voltage induced changes in the microwave response at 27 K. The effect of changes in the dielectric properties of the STO layer is less pronounced compared to those in the previous samples. The dip in the quality factor Q for positive voltage biases at 1–2 V is again strongly correlated to the changes in the dielectric constant ϵ_r of the STO layer. We observe that for negative voltage bias, which corresponds to adding electrons to the bottom YBCO film, both the resonant frequency f_0 and the quality factor Q decrease monotonically. This result complements the result for sample S2, in which case adding holes to the dominant YBCO layer resulted in an increase in both the resonant frequency f_0 and the quality factor Q. The magnitude of the effects is also comparable if one takes into account that STO in sample S3 is ~8 times thinner.

Since this sample showed a measurably large quality factor Q up to the normal state, we have also investigated how the field effect on the microwave response changes with temperature. Figure 17 shows the fractional change in the resonant frequency at six different temperatures. The frequency modulation at 14 K is almost identical to the one at 27 K. At 60 K, the modulation increases by about 20%. At 79 and 86 K the modulation is about 4 and 6 times larger than that at 14 K, respectively. We also notice that the scatter in the data points increases dramatically with temperature although we use identical averaging routines for each temperature measurement. This scatter might be due to small fluctuations in temperature or noise related to thermally activated processes. In the normal state of the YBCO film at 92 K, the scatter in the measurement is about 10^2 times larger than that at low temperatures. This noise makes the interpretation of the normal state frequency modulation data ex-

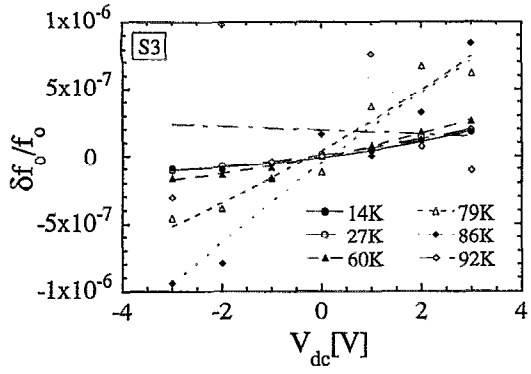

FIG. 17. Fractional changes in the resonant frequency vs applied dc voltage V_{dc} for sample S3 at six different temperatures [14 K (full circle), 27 K (open circle), 60 K (full triangle), 79 K (open triangle), 86 K (full diamond), 92 K (open diamond)].

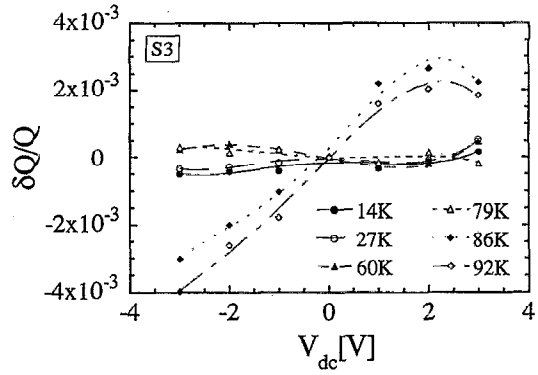

FIG. 18. Fractional changes in the quality factor vs applied dc voltage V_{dc} for sample S3 at six different temperatures [14 K (full circle), 27 K (open circle), 60 K (full triangle), 79 K (open triangle), 86 K (full diamond), 92 K (open diamond)].

tremely difficult. Nevertheless, a linear fit to this heavily scattered data seems to indicate that, on the average, the modulation might be very small.

In Fig. 18, the electric field induced fractional changes in the quality factor Q are shown at the same six temperatures used for the frequency measurements. Similar to the frequency measurements, the quality factor Q modulation is almost identical to 14 and 27 K. Curiously, the modulation changes sign but remains approximately equal in magnitude at 60 and 79 K. Close to T_c of the YBCO film at 86 and 92 K, the magnitude of the modulation increases by almost an order of magnitude compared to that at low- and mid-temperatures. Also, for positive voltage bias, the modulation shows strong nonlinearity which are again correlated to the changes in the dielectric constant ϵ_r of the STO film.

V. ANALYSIS OF RESULTS

In this section we will examine the results of the microwave measurements more closely and attempt to develop a semi-quantitative understanding of the dc electric field effects in these dielectric/superconductor layered structures. We will concentrate mostly on the behavior of samples S2 and S3 since they demonstrate, in part, regions of linearly modulated metallic response with no observable hysteresis. Results on sample S3 are potentially the most informative because, unlike sample S1, sample S3 does not show electrical hysteresis or large losses in its microwave response. Also, unlike sample S2, it has only one superconducting YBCO layer that can contribute to the microwave response in a wide range of temperatures.

In Table II, we list some key physical parameters of our samples. All the values listed in this table are estimates that are expected to be accurate to only within a factor of about 2. The effective surface resistance R_s values are determined from the measured quality factors Q's using Eq. (1). The effective surface reactance X_s values for samples S2 and S3 are determined under the assumptions of some simple models. In the case of S2, we use the linear fit in the inset of Fig. 12 and Eqs. (3) and (4). For S3, we expect a similar temperature dependence which is consistent with the standard 2-fluid model. However, instead of making a rather cumbersome 2-fluid fit to the whole frequency shift data shown in Fig. 15, we exploit the fact that at 82.5 K the surface resistance X_s should approximately equal the surface resistance R_s (since resonant frequency has a minimum at that temperature). Once we determine surface resistance X_s at 82.5 K, we work backwards and obtain the 25 K value for X_s using Eq. (3). dc voltage modulation of the surface reactance X_s and the surface resistance R_s at 25 K are calculated using the average of the hysteretic response for sample S1, and the quasi-linear regions for samples S2 and S3.

A. Sample S1

From the dc voltage dependence of Q and f_0 shown in Figs. 10 and 11, and the temperature dependence of these

TABLE II. The effective surface resistance R_s and reactance X_s at 25 and 82 K, and modulation of these quantities per applied dc voltage bias $\delta R_s/\delta V_{dc}$ and $\delta X_s/\delta V_{dc}$ at 25 K for the three trilayer samples S1, S2, and S3 (for modulation measurements, top layer is grounded, and quasi-linear regions are considered for samples S1 and S2).

Sample ID	R_s @25 K [Ω]	X_s @25 K [Ω]	R_s @82 K [Ω]	X_s @82 K [Ω]	$\delta R_s/\delta V_{dc}$ @25 K [μΩ/V]	$\delta X_s/\delta V_{dc}$ @25 K [μΩ/V]
S1	0.6	?	>0.8	?	+800 (hysteretic)	−2000 (hysteretic)
S2	0.04	0.25	0.5	2	−1	−8
S3	0.03	0.1	0.25	0.3	+4	+40

quantities under zero bias voltage shown in Fig. 9, we observe that the fractional changes in Q are related to those of f_0 by $\delta Q/Q \sim -10^3 \delta f_0/f_0$, where 10^3 is the scaling factor between resistive and reactive components of the response of the resonator given by X_{geo}/R_s. The response is nonmetallic since it does not seem to change sign with bias reversal (taking the offset voltage into account). Also, comparison of the low-frequency capacitance measurements with the microwave measurements indicates that there is a correlation between the changes of ϵ_r and those of f_0 which can be approximated by $\delta f_0/f_0 \sim -2\times10^{-5}\delta\epsilon_r/\epsilon_r$.

We believe, these results for sample S1 cannot be explained by mere changes of conductivity in a conventional normal or superconducting metallic layer(s). While we are not certain about the physical mechanism causing this overall behavior, one strong possibility is that the microwave response is dominated by the changes in the high frequency dielectric properties of the bulk of the thick STO layer. For an ionic dielectric material like STO, this effect might be very much dependent on the sample specific extrinsic properties of the STO thin film such as stress distribution and defect structure, and thus it is difficult to quantify. If we model the STO layer as a very lossy dielectric that dominates the microwave loss in the trilayer, then using the low quality factor Q we measure and the numerical analysis outlined in Sec. III we obtain an effective loss tangent value tan δ larger than 10^3 for the STO film. On the other hand, at 1 kHz capacitance measurements yield tan δ values $<10^{-1}$. Another model which is more plausible and consistent with both the low frequency capacitance and the microwave measurements includes a semiconductor-like region(s) in the trilayer structure. The symmetric suppression of ϵ_r in both polarities of voltage bias might indicate that the semiconductor-like region exists at both interfaces or within the STO layer. If we assume that the microwave loss and its voltage modulation are dominated by free carriers in the semiconductor-like region, then the corresponding surface density of carriers we obtain is $\sim 10^{15}$ carriers/cm^2.

B. Sample S2

In the analysis of microwave measurement results on sample S2, we will consider the regions in Fig. 14 below $V_{dc}<-10$ V where changes in STO properties can be neglected, and capacitance can be assumed to be constant. The analysis we present here closely resembles earlier published results except for the scaling of some measured quantities due to our new improved estimate of the geometric factor of the resonator.[9] From Eqs. (1)–(3) and our results from Fig. 14, we obtain $\delta R_s/\delta V_{dc} \sim -1$ $\mu\Omega$/V and $\delta X_s/\delta V_{dc} \sim -8$ $\mu\Omega$/V. The peak at $\sim$60 K for Q shown in Fig. 13 may represent the crossover temperature from dielectric to YBCO dominated loss or may result from a rather complicated interplay of leakage and dissipation of the microwave fields through the trilayer sample. Similar measurements of R_s on single films of YBCO which show comparable R_s values above 65 K give values less than 15 mΩ at 25 K. Thus, we will assume this value to be the upper bound for the effective surface resistance R_{sy} of the top YBCO film in the trilayer.

Figure 19 shows the modulation of the resonant frequency f_0 and the quality factor Q in terms of the dc electric field induced surface charge density δN. Induced surface charge density δN has been calculated using the formula $\delta N = \epsilon V/d$ where ϵ, V, and d are the dielectric constant calculated from the measured capacitance, the applied dc voltage, and the thickness of the STO layer, respectively. Solid lines are linear approximations to the data. Error bars denote statistical variations in the measured data.

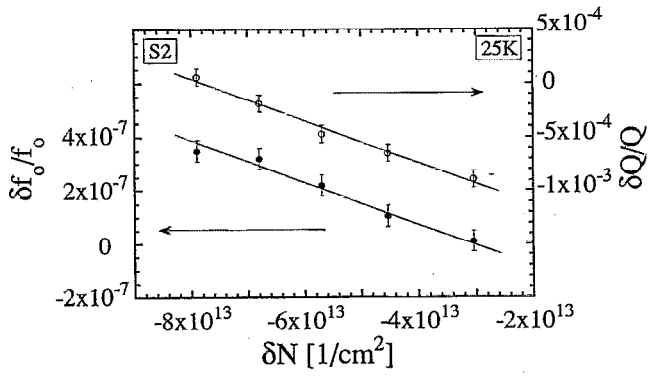

FIG. 19. Fractional changes in the resonant frequency and quality factor vs induced surface charge density δN at 25 K for sample S2 (solid lines are linear approximations to the data).

If we assume that the top YBCO layer dominates the microwave response, then the effective microwave surface impedance $Z_s^{\text{thin-film}}$ in the thin film limit is given by

$$Z_s^{\text{thin-film}} = R_s^{\text{thin-film}} + iX_s^{\text{thin-film}} = \frac{1}{(\sigma_r - i\sigma_i)t_3}, \tag{5}$$

where σ_r and σ_i are the real and imaginary parts of the conductivity, respectively, and t_3 is the thickness of the top YBCO film.

In the 2-fluid model, the frequency dependent complex conductivity is related to the density of normal and superconducting carriers of the YBCO film.[26] At 25 K, our sample is in the thin film limit where the penetration depth is larger than the thickness of the top superconducting film, and also $R_{sy} \ll X_{sy}$. Thus,

$$Z_s^{\text{thin-film}} = 1 \Big/ \left(\frac{N_n e^2 \tau}{m_n} - i\,\frac{N_s e^2}{2\pi f m_s}\right) \sim \frac{N_n e^2 \tau}{m_n} \Big/ \left(\frac{N_s e^2}{2\pi f m_s}\right)^2 + i1 \Big/ \frac{N_s e^2}{2\pi f m_s}, \tag{6}$$

where $N_n(N_s)$ is the areal number density of normal (superconducting) carriers, e is the unit electric charge, $m_n(m_s)$ is the effective mass of normal (superconducting) carriers, τ is the relaxation time for normal carriers, and f is the frequency of applied electromagnetic field.

With the approximation $m_n \sim m_s$,[11] and the assumption $Z_{sy} \sim Z_s^{\text{thin-film}}$, the linear relation between the fractional changes of Z_{sy} and of the density of carriers in the film simplifies to

$$\delta R_{sy}/R_{sy} \sim \delta N_n/N_n - 2\,\delta N_s/N_s, \tag{7}$$

$$\delta X_{sy}/X_{sy} \sim -\,\delta N_s/N_s. \tag{8}$$

We note that for dc measurements in the normal state one expects $\delta R/R \sim -\delta N_n/N_n$.[5] From the capacitance measurements, we can calculate the induced charge density δN at the interface of the top YBCO layer. Assuming a bulk charge carrier density of 5×10^{21} carriers/cm^3 for the YBCO film, we obtain for the fractional areal charge density change per applied dc volt $(\delta N/N)/\delta V_{dc} \sim -3\times10^{-5}$ V^{-1}.

Comparison of this change with corresponding fractional changes in Z_{sy} of the top YBCO film yields $\delta X_{sy}/X_{sy} \sim -\delta N/N$ and $\delta R_{sy}/R_{sy} \sim -2\delta N/N$ at 25 K. The $\delta X_{sy}/X_{sy}$ result implies that roughly all the charges induced at the interface due to the applied dc electric field go into the superconducting state. If we assume that our estimate of R_{sy} is reasonably accurate, then our result for $\delta R_{sy}/R_{sy}$ further implies that the fractional changes in N_n are smaller than those in N_s. One possible explanation for the apparent smaller fractional change in N_n is that the effective normal carrier density in the system at low temperatures is dominated by normal carriers other than the intrinsic ones predicted by the simple 2-fluid theory, such as the extrinsic normal carriers in normal inclusions in the film.

C. Sample S3

We will use a simple multilayer thin film model in the analysis of measurement results on sample S3. We expect the thin film approximation to work reasonably well since; the top Au layer is much thinner than the microwave skin depth so that the microwave fields can penetrate through this layer, the intermediate STO layer is thin and does not show large (hysteretic) losses, and the bottom YBCO layer is thick enough so that microwave field leakage through the substrate is limited but thin enough to have approximately uniform current density across its thickness.

In this model, the effective microwave surface impedance $Z_s^{\text{thin-film}}$ in the thin film limit for the trilayer sample is given by

$$Z_s^{\text{thin-film}} = R_s^{\text{thin-film}} + iX_s^{\text{thin-film}} = \frac{1}{g_1+g_2+g_3+g_{\text{leak}}}, \quad (9)$$

where g_1, g_2, and g_3 are the surface conductivities for the bottom YBCO, intermediate STO, and top Au, respectively. g_{leak} is the contribution of the microwave field leakage through the substrate (and may also include a contribution due to the radiation losses in the cavity) to the total surface conductance.

The YBCO surface conductivity g_1 in the thin film limit is given by

$$g_1 = (\sigma_r - i\sigma_i)t_1, \quad (10)$$

where σ_r, σ_i, and t_1 are the normal and imaginary parts of the conductivity, and the thickness of the film, respectively.

If we consider the intermediate STO layer as a lossy dielectric medium, then the surface conductivity g_2 can be written in the form[27]

$$g_2 = i2\pi f\epsilon_0\epsilon_r(1 - i\tan\delta)t_2, \quad (11)$$

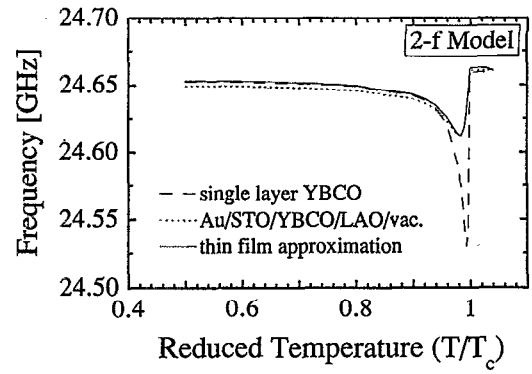

FIG. 20. Resonant frequency vs reduced temperature predicted by a single layer YBCO model (dashed line), a trilayer model in the thin film approximation (solid line), and a full multilayer model from Fig. 8 (dotted line).

where f is the frequency of the applied electromagnetic field, ϵ_0 is the permittivity of free space, and ϵ_r, $\tan\delta$ and t_2 are the relative permittivity, the loss tangent, and the thickness of the film, respectively.

Since Au is a normal metal with high electrical conductivity, the surface conductivity in the thin film limit simplifies to

$$g_3 = \sigma_{\text{Au}} t_3, \quad (12)$$

where σ_{Au} and t_3 are the conductivity and the thickness of the film, respectively.

Figures 20 and 21 illustrate how the predictions of a single layer YBCO model (dashed line) and thin film approximation for the trilayer presented above (solid line) compare with that of a more detailed trilayer model (dotted line) which makes full use of the multilayer model presented in Fig. 8. In Figs. 20 and 21, we assume that a simple 2-fluid-like complex conductivity of the YBCO layer is the only parameter that changes with time for all three models. The estimates we have used for the various parameters related to these models are obtained from either the results of our measurements or standard reference books. Since these figures are just for qualitative illustration purposes, we will not go into the details except that the parameter g_{leak} in Eq. (9)

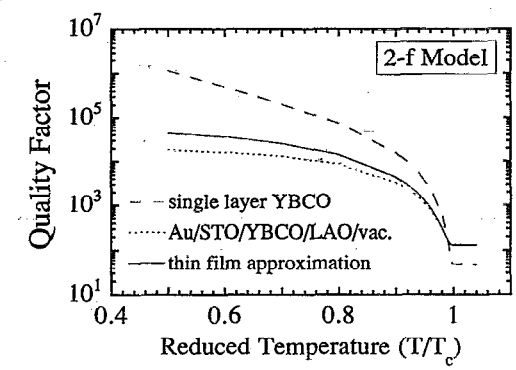

FIG. 21. Quality factor vs reduced temperature predicted by a single layer YBCO model (dashed line), a trilayer model in the thin film approximation (solid line), and a full multilayer model from Fig. 8 (dotted line).

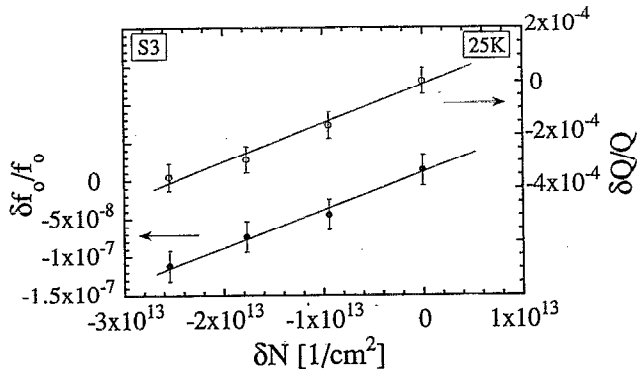

FIG. 22. Fractional changes in the resonant frequency and quality factor vs induced surface charge density δN at 27 K for sample S3 (solid lines are linear approximations to the data).

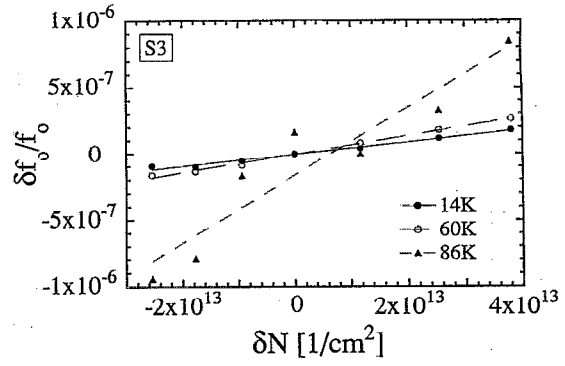

FIG. 23. Fractional changes in the resonant frequency vs induced surface charge density δN for sample S3 at three different temperatures; 14 K (full circle), 60 K (open circle), 86 K (full triangle) (lines are guide to the eye).

includes only the leakage through the substrate and has been estimated to be $\sim 0.03+i0.03\ \Omega^{-1}$ by using the formalism shown in Fig. 8 for the substrate and the vacuum behind it. From these figures, we observe that the thin-film-approximation predictions are reasonably good, particularly at higher temperatures. Also, we clearly see that the effects of a normal conducting layer parallel to YBCO are mainly to increase the loss at low temperatures, decrease the loss when the superconducting film goes into the normal state, and reduce the dip in the frequency response.

At low temperatures, we expect the surface inductance due to superconducting YBCO to dominate the total conductance of the trilayer. Also, using the data given in Table II and assuming that the changes in the dielectric properties of the STO layer at low temperatures and large negative voltage biases are negligible,[28] the fractional changes in $Z_s^{\text{thin-film}}$ can be simplified to read

$$\frac{\delta X_s^{\text{thin-film}}}{X_s^{\text{thin-film}}} \sim -\frac{\delta(\sigma_i t_1)}{\sigma_i t_1} \sim -\frac{\delta(N_s)}{N_s}, \tag{13}$$

and

$$\frac{\delta R_s^{\text{thin-film}}}{R_s^{\text{thin-film}}} \sim \frac{\delta(\sigma_r t_1+\sigma_{\text{Au}} t_3)}{\sigma_r t_1+\sigma_{\text{Au}} t_3} - 2\,\frac{\delta(\sigma_i t_1)}{\sigma_i t_1} \sim -2\,\frac{\delta(N_s)}{N_s}, \tag{14}$$

where we have used the relations given in Eq. (6) for the complex conductivity $\sigma_r+i\sigma_i$ of the YBCO film. We have further simplified the expression in Eq. (14) since we expect surface conductivity of Au to be much larger than that of the normal channel of the superconducting YBCO film at low temperatures. Here, we notice that due to the existence of a parallel channel of normal conductor Au, changes in N_n are negligible compared to those in N_s in the determination of the surface resistance modulation as given by Eq. (14) [cf. Eq. (7)].

Predictions of the Eqs. (13) and (14) are consistent with the microwave modulation results. Figure 22 shows the modulation of the resonant frequency f_0 and the quality factor Q for sample S3 at 27 K as a function of the field induced surface charge density δN below -2×10^{13}. δN has been calculated from the measured capacitance as described before. We see that, under these conditions, both the quality factor and the resonant frequency decrease approximately linearly when positive charges are depleted from the bottom YBCO film. If we assume that the density of carriers in the YBCO film is $\sim 5\times10^{21}$ cm^{-3}, and that the carriers are mostly in the superconducting state at 27 K (similar to what we assumed for sample S2), then the results show that, within a factor of two, most holes filled at the interface due to the applied electric field are from the superconducting channel, i.e., $\delta N_s \sim \delta N$, complementing the results obtained for sample S2.

Figure 23 and 24 show the modulation of the resonant frequency f_0 and the quality factor Q as a function of electric field induced surface charge density δN at three different temperatures (14, 60, and 86 K). From the frequency modulation data shown in Fig. 23, we see that the magnitude of the modulation increases by less than 50% from 14 to 60 K, but more than a factor of 5 from 14 to 86 K. The quality factor modulation data in Fig. 24 show that the modulation of the quality factor does not change much for positive bias but reverses sign for the negative bias from 14 to 60 K. From 14 to 86 K, the quality factor modulation increases by more than a factor of 5, and also for positive bias the curvature changes from concave-up to concave-down.

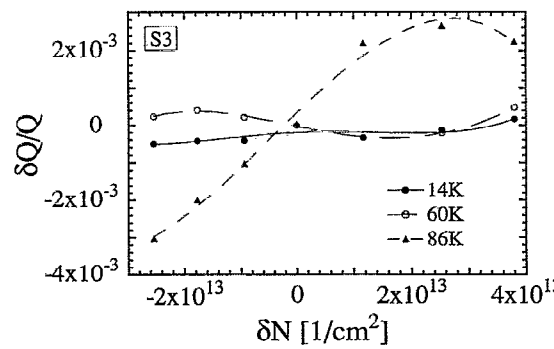

FIG. 24. Fractional changes in the quality factor vs induced surface charge density δN for sample S3 at three different temperatures; 14 K (full circle), 60 K (open circle), 86 K (full triangle) (lines are guide to the eye).

At high enough temperatures, the number of superconducting carriers in the YBCO film becomes so small that the inductance related to it becomes negligible compared to the conductance related to the normal carriers in the YBCO and Au films. Under this condition, similar to Eqs. (13) and (14), the fractional changes in $Z_s^{\text{thin-film}}$ in this limit then becomes

$$\frac{\delta R_s^{\text{thin-film}}}{R_s^{\text{thin-film}}} \sim -\frac{\delta(\sigma_r t_1 + 1.4\epsilon_r \tan\delta\, t_2 + \sigma_{\text{Au}} t_3)}{\sigma_r t_1 + 1.4\epsilon_r \tan\delta\, t_2 + \sigma_{\text{Au}} t_3}, \quad (15)$$

and

$$\frac{\delta X_s^{\text{thin-film}}}{X_s^{\text{thin-film}}} \sim \frac{\delta(\sigma_i t_1 - 1.4\epsilon_r t_2 - 0.03)}{\sigma_i t_1 - 1.4\epsilon_r t_2 - 0.03} - 2\,\frac{\delta(\sigma_r t_1 + 1.4\epsilon_r \tan\delta\, t_2 + \sigma_{\text{Au}} t_3)}{\sigma_r t_1 + 1.4\epsilon_r \tan\delta\, t_2 + \sigma_{\text{Au}} t_3}. \quad (16)$$

Low-frequency measurements of the dielectric properties of the STO layer show that the dielectric constant ϵ_r and the loss tangent $\tan\delta$ do not change appreciably between 10 and 100 K. Therefore, it is difficult to attribute the enhanced modulation at 86 K to the simple modulation effects in the STO layer. Also, the fractional modulation in the Au layer is expected to be much smaller than that in the YBCO layer on basic grounds that the surface conductivity of Au is comparable if not larger than the normal component of that of the YBCO layer at any temperature and the density of carriers in Au is >10 times larger than that in YBCO. As a result, we believe that the large enhancement of the modulation with temperature for this sample cannot be explained within the simple formalism we have developed above.

D. Discussion and summary

One way to improve the above formalism would be to retain the general relations established between the surface conductivities of different layers and the effective surface impedance $Z_s^{\text{thin-film}}$, but improve models that relate the surface conductivities to some physical parameters. For example, one may include the carrier density dependence of the superconducting transition temperature in the expression that relates the surface conductance of YBCO to the density of carriers. This would enhance the modulation close to the transition temperature. Another plausible model might include other modulation effects, such as the ion motion under electric field, in addition to the electronic charge modulation. Electric field induced motion of oxygen ions in YBCO could change the effective density of carriers,[29] which in turn would change the effective surface conductivity of the film. Also, similar motion of oxygen ions in the STO film[30,31] might change the microwave response of this ionic dielectric material. These effects would most probably be thermally activated, and hence can describe the observed temperature dependence of the field modulation. Nevertheless, since the formalism we have used in the analysis has many parameters and the experimental data for the temperature dependence of the microwave response are limited, we will not pursue the plausibility of the various mechanisms we have outlined in this paragraph any further.

In summary, our analysis of the results indicates that the electric field induced changes in *both* the dielectric properties of the gate dielectric (STO) and the complex conductivity of the superconducting channel (YBCO) contribute to the microwave response. Large hysteretic modulation effects ($\sim 10^3$ $\mu\Omega$/V) were obtained for a Au/STO/YBCO sample (S1) that showed reduced transition temperature T_c (~80 K) for the YBCO layer and hysteretic low-frequency dielectric properties for the STO layer. At low temperatures (<50 K) and large electric fields ($<10^7$ V/m), a better quality YBCO/STO/YBCO sample (S2) showed a linearly decreasing surface resistance and reactance with voltage bias ($\sim\mu\Omega$/V). A simple 2-fluid analysis in the thin film limit indicated that this modulation can be explained in terms of field induced superconducting hole filling in the top YBCO film. Another good quality sample (S3) with Au/STO/YBCO configuration showed linearly increasing surface resistance and reactance with voltage bias (~10 $\mu\Omega$/V) at low temperatures (<50 K). A similar 2-fluid analysis in the thin film limit indicated that the response can be explained in terms of field induced superconducting hole depletion in the bottom YBCO film. For samples S2 and S3, the fractional surface resistance and surface reactance modulation ($\delta R_s/R_s$ and $\delta X_s/X_s$) were of the order of fractional surface charge density modulation ($\delta N/N$) in the dominant YBCO layer (at present, the largest $\delta N/N$ we have achieved is 10^{-3}). Additional analysis of the results indicates that the modulation of the microwave surface impedance at low temperatures is dominated by the charge density modulation in the superconducting channel $\delta N_s/N_s$, most likely due to the existence of external or extrinsic channels of normal carriers in the samples which show weaker field dependence. At higher temperatures (>50 K), sample S3 showed larger modulations ($\sim 10^2$ $\mu\Omega$/V) that cannot be explained with the simple models utilized in this article.

VI. CONCLUSION

We have studied the effect of dc electric field on the effective microwave surface impedance Z_s of (Au)/STO/YBCO and YBCO/STO/YBCO trilayers, fabricated *in situ* by PLD. Low-frequency (~kHz) and dc electrical properties of the samples were measured to obtain critical transition temperature T_c of YBCO, and temperature and electric field dependent dielectric properties of STO films. Microwave properties of the samples were determined using a dielectric resonator technique at 26 GHz. Large induced surface charge densities δN of 10^{14} cm^{-2} over an area of about 1 cm^2 were achieved in the trilayer films by applying dc voltages (with corresponding electric fields of up to 10^8 V/m) between the top and bottom conducting layers. Field modulation effects on the microwave response of the samples were measured at various temperatures (14–92 K) and electric fields ($\pm 10^8$ V/m). Samples with different electrical and structural characteristics were prepared to investigate field modulation effects over differing magnitudes (1 $\mu\Omega$/V–10^3 $\mu\Omega$/V). The microwave results were analyzed using simple models that incorporate multilayer structures with parallel conducting and insulating channels in the thin-film limit.

We observe that the microwave properties of *both* superconducting YBCO and insulating STO change under dc electric fields. Field effect studies at low temperatures ($T<T_c/2$) show that under certain bias conditions where the dielectric properties of the STO layer saturate, changes in the microwave response of the sample can be explained in terms of charge modulation effects in the dominant YBCO layer. Adding holes into (extracting holes from) the dominant YBCO layer result in linear reduction (increase) in the microwave surface resistance R_s and surface reactance X_s. These studies also indicate that the modulation of the microwave surface impedance at low temperatures is mainly due to charge density modulation in the superconducting channel $\delta N_s/N_s$, i.e., $\delta N_s/N_s \gg \delta N_n/N_n$. One likely explanation for this result is that in the trilayer structure there are external or extrinsic channels of normal carriers, such as normal carriers in the top Au layer in the case of Au/STO/YBCO trilayers or normal inclusions in the films in general, which show weaker field modulation. At temperatures close to T_c, we observe about an order of magnitude larger modulation effects on the microwave response which cannot be explained within the framework of the models used in this article.

From a technological point of view, electric field modulation of surface impedance may open new opportunities for novel active superconducting microwave devices.[9] The potential for practical microwave device applications depends on various specific requirements such as the impedance level, speed, input-output isolation, and the magnitude of the absolute and fractional modulation of the microwave response.[32] The fractional modulation of the microwave response ($\delta R_s/R_s$ and $\delta X_s/X_s$) is of the order of fractional surface charge density modulation $\delta N/N$, similar to the dependence of the low-frequency modulation of the normal state resistance $\delta R_n/R_n$ and the superconducting state kinetic inductance $\delta L_s/L_s$ on the surface carrier density modulation $\delta N/N$. Therefore, most of the issues that have been addressed in low-frequency field effect devices can be examined in an analogous manner in microwave field effect devices.[1–8] However, due to the increased importance of electromagnetic field penetration and radiation at high frequencies, one needs to meet more stringent requirements for devices that operate at microwave frequencies. For a generic field-tunable device structure, for example, where it is important to have extremely low total microwave loss (i.e., low resistive loss and limited microwave field leakage through the multilayer structure), one needs low temperature (well below T_c) operation and rather thick ($\geq\lambda/5$) YBCO layer(s). These conditions, in particular the need to use relatively thick YBCO film, place an upper-bound of about 10^{-2} for the maximum fractional microwave response modulation we can achieve with YBCO/STO-based devices using our existing materials technology. If one can tolerate larger microwave loss in the device, then larger fractional modulation effects can be achieved by either operating the device close to the T_c of the superconducting layer(s),[33] or using a different device geometry where microwave fields are concentrated in the dielectric layer and the modulation is dominated by changes in the dielectric constant of that layer.[34]

ACKNOWLEDGMENTS

We acknowledge fruitful discussions with Professor F. C. Wellstood, J. Booth, M. Pambianchi, and Y. Gim.

[1] J. Mannhart, J. G. Bednorz, K. A. Mueller, and D. G. Schlom, Z. Phys. B **83**, 307 (1991).
[2] X. X. Xi, Q. Li, C. Doughty, C. Kwon, S. Bhattacharya, A. T. Findikoglu, and T. Venkatesan, Appl. Phys. Lett. **59**, 3470 (1991).
[3] J. Mannhart, D. G. Schlom, J. G. Bednorz, and K. A. Muller, Phys. Rev. Lett. **67**, 2099 (1991).
[4] Y. Gim, C. Doughty, X. X. Xi, A. Amar, T. Venkatesan, and F. C. Wellstood, Appl. Phys. Lett. **62**, 3198 (1993).
[5] X. X. Xi, C. Doughty, A. Walkenhorst, C. Kwon, Q. Li, and T. Venkatesan, Phys. Rev. Lett. **68**, 1240 (1992).
[6] J. Mannhart, J. Strobel, J. G. Bednorz, and Ch. Gerber, Appl. Phys. Lett. **62**, 630 (1993).
[7] X. X. Xi, C. Doughty, A. Walkenhorst, S. N. Mao, Qi Li, and T. Venkatesan, Appl. Phys. Lett. **61**, 2353 (1992).
[8] A. Jaeger, J. C. Villegier, P. Bernstein, J. Bok, and C. Force, IEEE Trans. Appl. Supercond. **3**, 2933 (1993).
[9] A. T. Findikoglu, C. Doughty, S. M. Anlage, Q. Li, X. X. Xi, and T. Venkatesan, Appl. Phys. Lett. **63**, 3215 (1993).
[10] See, for example, N. Newman and W. G. Lyons, J. Supercond. **6**, 119 (1993).
[11] A. T. Fiory, A. F. Hebard, R. H. Eick, P. M. Mankiewich, R. E. Howard, and M. L. O'Malley, Phys. Rev. Lett. **65**, 3441 (1990).
[12] See, for example, A. Inam, M. S. Hegde, X. D. Wu, T. Venkatesan, P. England, P. F. Miceli, E. W. Chase, C. C. Chang, J. M. Tarascon, and J. B. Wachtman, Appl. Phys. Lett. **53**, 908 (1988).
[13] A. T. Findikoglu, C. Doughty, S. Bhattacharya, Qi Li, X. X. Xi, T. Venkatesan, R. E. Fahey, A. J. Strauss, and Julia M. Phillips, Appl. Phys. Lett. **61**, 1718 (1992).
[14] See, for example, R. J. Cava, A. W. Hewat, E. A. Hewat, B. Batlogg, M. Marezio, K. M. Rabe, J. J. Krajewski, W. F. Peck, Jr., and L. W. Rupp Jr., Physica C **165**, 419 (1990).
[15] Samples where the top YBCO layer is deposited at higher temperatures show significant degradation in the breakdown characteristics of the intermediate STO layer.
[16] R. Waser, T. Baiatu, and K. Hardtl, J. Am. Ceram. Soc. **73**, 1645 (1990).
[17] T. Hirano, M. Ueda, K. Matsui, T. Fujii, K. Sakuta, and T. Kobayashi, Jpn. J. Appl. Phys. **31**, 11345 (1992).
[18] A. Walkenhorst, C. Doughty, X. X. Xi, S. N. Mao, Q. Li, T. Venkatesan, and R. Ramesh, Appl. Phys. Lett. **60**, 1744 (1992).
[19] N. Klein, U. Dahne, U. Poppe, N. Tellmann, K. Urban, S. Orbach, S. Hensen, G. Muller, and H. Piel, J. Supercond. **5**, 195 (1992).
[20] N. W. Ashcroft and N. D. Mermin, *Solid State Physics* (Saunders College Press, Philadelphia, PA, 1976), p. 5.
[21] We measure Q of about 30000 for good quality 80-nm-thick YBCO films at 25 K.
[22] R. C. Neville, B. Hoeneisen, and C. A. Mead, J. Appl. Phys. **43**, 2124 (1972).
[23] See the inset to Fig. 12.
[24] The decrease in Q with temperature at low temperatures is mainly due to increase in the density of carriers in the normal channel (i.e., quasiparticles).
[25] C. J. Gorter and H. B. G. Casimir, Physik Z **35**, 963 (1934).
[26] H. London, Proc. R. Soc. London Ser. A **176**, 522 (1940).
[27] S. Y. Liao, *Microwave Devices and Circuits* (Prentice-Hall, Englewood Cliffs, NJ, 1985), p. 36.
[28] At large electric fields, STO dielectric constant for all three samples seems to saturate at around the same value (see Fig. 5).
[29] N. Chandrasekhar, Oriol T. Valls, and A. M. Goldman, Phys. Rev. Lett. **71**, 1079 (1993).
[30] L. C. Walter and R. E. Grace, J. Phys. Chem. Solids **28**, 239 (1967).
[31] N. H. Chan, R. K. Sharma, and D. M. Smyth, J. Electrochem. Soc. **128**, 1762 (1981).
[32] See, for example, R. W. Babbitt, T. E. Koscica, and W. C. Drach, Microwave J. **6**, 63 (1992).
[33] See the microwave results (close to T_c) on sample S3 in Sec. V.
[34] A. T. Findikoglu, T. Nakamura, H. Tokuda, and M. Iiyama, Rev. Sci. Instrum. (to be published).